Novel ultrahard carbon allotropes from crystal chemistry and first principles: rhombohedral ene-C21 and yne-C24

Samir F. Matar, Vladimir Solozhenko

Novel ultrahard carbon allotropes from crystal chemistry and first principles: rhombohedral *ene*-C_{21} and *yne*-C_{24}

Samir F. Matar [1] and Vladimir L. Solozhenko [2,*]

[1] *Lebanese German University (LGU), Sahel Alma, Jounieh, Lebanon*

https://orcid.org/0000-0001-5419-358X

[2] *LSPM–CNRS, Université Sorbonne Paris Nord, 93430 Villetaneuse, France*

https://orcid.org/0000-0002-0881-9761

Abstract

Rhombohedral *ene*-C_{21} and *yne*-C_{24}, characterized by the presence of C=C and C≡C bonds, respectively, inserted into the 9R diamond polytype C_{18}, are proposed as novel ultrahard carbon allotropes from crystal chemistry and first principles. Like 9R C_{18}, they belong to the **cfe** topology characteristic of layered SiC polytypes. With ultrahard properties approaching those of diamond and lonsdaleite, *ene*-C_{21} and *yne*-C_{24} are dynamically stable with phonon signatures identifying C=C and C≡C high frequency vibrations similar to molecular allene and acetylene. The electronic band structures correspond to insulating C_{18}, metallic *ene*-C_{21} and semiconducting *yne*-C_{24}.

Keywords: diamond polytypes; hybridization; DFT; hardness; phonons; electronic structure

* Corresponding author (vladimir.solozhenko@univ-paris13.fr)

Introduction

Diamond, known mainly in the cubic form, has a less common hexagonal form called lonsdaleite. Such structures are also observed in binary SiC, and the different phases are called polytypes, which are distinguished by the stacking of layers, usually labeled A/B/C: AB in 2H (2 layers; hexagonal system), ABC in 3C (3 layers; cubic system), ABCB in 4H (4 layers; hexagonal system), etc. [1]. Silicon and carbon are isoelectronic with respect to the valence shell, and diamond has analogous polytypes, with the best known being 3C, which corresponds to cubic diamond, and 2H, which corresponds to lonsdaleite. Other diamond polytypes: 4H, 8H, 9R to 21R (R for rhombohedral) have been identified with calculated X-ray diffraction data published by Ownby *et al.* in 1992 [2]. Recently, it has been shown that a novel class of machine-learning-based interatomic potentials can be used for random structure search and readily predicts several hitherto unknown carbon allotropes [3], allowing them to be identified with topology labels such as **dia** (diamond), **lon** (lonsdaleite), and for polytypes: **cfc** for 4H diamond, **cfe** for rhombohedral 9R. In view of the enormous number of carbon allotropes, experimentally found and theoretically predicted, a database "SACADA" has been created to store them with topologies and identifiers; 9R allotrope (hRC_{18} in Pearson notation) studied here and classified with **cfe** topology and database code: 447 [4].

In 3C and 2H diamond, as well as in the extended lattice polytypes, the valence 4 electrons ($2s^2$, $2p^2$) arrange in tetrahedra with sp^3-like hybridization; note that this term, as well as other carbon hybridizations (sp^2 and sp^1), are common in organic chemistry, and less so in the solid state chemistry; nevertheless, they are useful for establishing the chemical description of the bonding and the resulting physical and chemical properties.

For applications such as electronics, the physical properties of diamond can be modified by introducing trigonal C(sp^2) - double C=C bonds as in ethene - and linear C(sp^1) - triple C≡C bonds as in acetylene - on the one hand, and by working on the particle size as in nanodiamonds, on the other hand. Indeed, recent works have shown that nanodiamonds with mixed C(sp^2)-C(sp^3) hybridization play an important role in designing advanced electronic materials [5]. Zhai *et al*. highlighted electrochemical applications of hybrid diamond/sp^2-C nanostructures [6]. Furthermore, regarding other mixed carbon hybridizations, sp^3-sp^1 were recently identified in superhard so-called "*yne*-diamond", which is classified as semi-metallic [7].

In this context, we considered the reduction of the sp^2/sp^3 extended stoichiometries allotropes, and C_{10}, C_{14} and C_{18} were proposed as derived respectively from 4H, 6H and 8H diamond polytypes, respectively, and also characterized by ultrahardness close to diamond, and semi-metallic electronic structure due to the presence of C(sp^2) [8]. The purpose of the present work was to study the changes in the mechanical and electronic properties of **cfe** 9R (hRC_{18}) allotrope, referred to as C_{18} in the present work, by the insertion of sp^2 and sp^1 carbon atoms in two stoichiometries, based on crystal chemistry rationale and subsequent first-principles ground state energy calculations of stable structures and derived quantities within the well-established quantum mechanics framework of the density functional theory DFT [9,10]. The two novel allotropes: *ene*-C_{21} with sp^3-sp^2 mixed

hybridizations and *yne*-C_{24} with sp^3-sp^1 mixed hybridizations retain the same **cfe** topology of the original C_{18}. *ene*-C_{21} and *yne*-C_{24} were found unique from the CCDC curation and provided with corresponding DOI references [11,12].

Brief presentation of the computational framework

The methodology was developed in earlier work (cf. [8] and the papers cited therein). Essentially, the search for the ground state structures with minimal energies was performed with unconstrained geometry optimizations within the DFT-based plane-wave Vienna Ab initio Simulation Package (VASP) [13] using the projector augmented wave (PAW) method for potentials [14]. Within the DFT, the effects of exchange and correlation (XC) were treated using Generalized Gradient Approximation (GGA) scheme [15]. Investigation of the mechanical properties was based on the calculations of the elastic properties by performing finite distortions of the lattice and deriving the elastic constants from the strain-stress relationship. The calculated elastic constants C_{ij} were then used to obtain the bulk (*B*) and the shear (*G*) moduli using the Voigt averaging method [16] based on uniform strain. Besides the mechanical properties, the dynamic stability was determined from the calculations of the phonons and illustrated with the corresponding band structures in the reciprocal space (Brillouin zone) using the "Phonopy" interface code based on the Python language [17]. The structures were plotted using the VESTA graphical program [18]. For the evaluation of the electronic properties, the band structures were obtained with the all-electrons augmented spherical wave method ASW [19].

Crystal chemistry results

The 9R diamond polytype (hRC_{18}; space group *R*-3*m* No. 166) is shown in Fig. 1a, in two representations: ball and stick (left) and tetrahedral stacking (right). *C4* tetrahedra are corner sharing within 9 layers like 9-layered SiC polytype. Table 1 listes the structural parameters showing agreement between literature and presently calculated values of the lattice constants and the z values of three (6c) 0,0,z sites. The shortest C-C separations have two d(C-C) values: 1.54 Å and 1.56 Å, in contrast to diamond with a unique d(C-C) =1.54 Å. Nevertheless, the close relationship to diamond is established by the identical cohesive energy of E_{coh} = 2.479 eV/atom.

The introduction of a trigonal sp^2 carbon was achieved by inserting of a 4^{th} carbon at the (3a) 0,0,0 site resulting in a C_{21} stoichiometry. The resulting constrained structure with short C-C distances was relaxed along successive cycles of geometry optimization until reaching the ground state configuration whose parameters are shown in Table 1, 2^{nd} column, characterized by the shortest distance: 1.46 Å assigned to the C=C bond, larger by 0.11 Å than that in the ethylene molecule (~1.35 Å). The perturbation of the 9R diamond polytype (hRC_{18}) leads to a decrease of the cohesive energy E_{coh} = 2.061 eV/atom. The structure shown in Fig. 1b exhibits a different stacking of tetrahedra and a less compact structure quantified by the decrease in density from ρ = 3.52 g/cm^3 in

C_{18} to 3.39 g/cm^3 in C_{21}. Note that the configuration of sp^2 carbon in the present *ene*-C_{21} with C-C-C motifs is closer to the propadiene C_3H_4 molecule, $H_2C{=}C{=}CH_2$.

To create the carbon allotrope with C≡C bonds, the (3a) 0,0,0 position of *ene*-C_{21} was changed to (6c) 0,0,z resulting in a C_{24} stoichiometry. Following the same geometry relaxation protocol as above, the final structure with zero strains is shown in Fig. 1c and the lattice parameters are given in Table 1, 3rd column. As expected, the structure is now characterized by a very short C-C distance of 1.21 Å, close to that observed in the acetylene molecule. The more open structure in Fig. 1c, with a different arrangement of the *C4* tetrahedra, has a low density $\rho = 3.13$ g/cm^3. The cohesive energy is reduced by an order of magnitude E_{coh}/atom = -1.923 eV. The two novel *ene*-C_{21} and *yne*-C_{24} allotropes have been identified with **cfe** topology like original C_{18}.

Charge density projections

A further qualitative illustration of the different types of hybridization is obtained from the projections of the charge densities. Figs 2a, 2b and 2c, which reproduce the crystal structure sketches of Fig. 1, highlight the volumes shown in yellow. In diamond-like C_{18} (Fig. 2a), the sp^3-type hybridization is clearly observed from the tetrahedral volumes around the C atoms. Like diamond, the rhombohedral 9R polytype is a perfectly covalent system with similar physical properties (mechanical, dynamic, etc.) and electronic structure as shown below. Changes are observed in the hybrid *ene*-C_{21} (Fig. 2b), where the sp^3-type hybridization is now accompanied by the sp^2-type one observed with the yellow volumes along the C-C-C unit aligned along the vertical hexagonal *c*-direction. In Fig. 2c, representing the projections in *yne*-C_{24}, besides the sp^3 tetrahedral shapes, a remarkable charge density is observed along the aligned C-C-C-C unit with strong localization for the middle C-C clearly featuring the C≡C triple bond. Therefore, the mixed hybridized novel allotropes are further illustrated by the charge density projections.

Mechanical properties

The evaluation of the mechanical properties was carried out by calculating the elastic properties by performing finite distortions of the lattice. The elastic constants C_{ij} were then derived from the strain-stress relationship, assuming statistically isotropic solid on a large scale. The C_{ij} were then used to obtain the bulk (*B*) and shear (*G*) moduli using the Voigt averaging method [16].

The calculated sets of elastic constants are given in Table 2. All C_{ij} values are positive, and their combinations obey the rules of mechanical stability of the system:

$$C_{11} > |C_{12}|;\ (C_{11}+C_{12})\cdot C_{33} > 2C_{13}^2;\ C_{44} > 0;\ C_{66} > 0$$

The bulk (*B*) and shear (*G*) moduli were calculated from elastic tensors within the Voigt averaging scheme using ELATE software [20]. Diamond-like C_{18} has the largest B_V and G_V close to the

accepted values for diamond (B_V = 445 GPa and G_V = 550 GPa [21]). For hybrid C_{21}, large B_V and G_V are obtained but they are of smaller magnitudes compared to the original polytype. The trend of smaller B_V and G_V is confirmed for C_{24}. The two hybrid systems with lower densities are increasingly more compressible.

Vickers hardness (H_V) has been predicted using four modern theoretical models. The thermodynamic (T) model [22], which is based on thermodynamic properties and crystal structure, shows surprising agreement with available experimental data [23] and is therefore recommended for hardness evaluation of superhard and ultrahard phases [24]. The Lyakhov-Oganov (LO) approach [25] takes into account the topology of the crystal structure, the strength of covalent bonding, the degree of ionicity and directionality; however, in the case of ultrahard phases of light elements, this model gives underestimated hardness values [23,24]. Two empirical models, Mazhnik-Oganov (MO) [26] and Chen-Niu (CN) [27], use the elastic properties. Fracture toughness (K_{Ic}) has been evaluated within the Mazhnik-Oganov model [26]. The results for the currently proposed hexagonal carbon allotropes and others from the literature are summarized in Tables 3 and 4.

Table 3 shows the crystal parameters, density and Vickers hardness obtained from the thermodynamic model. For pristine C_{18}, the values of density (ρ), hardness (H_V) and bulk modulus (B_0) have magnitudes close to those of diamond and lonsdaleite. This is quite expected since 9R carbon is considered to be a diamond polytype. The two hybrid allotropes show lower values closer to C_{18}.

Table 4 displays the hardness values along the different models in addition to the thermodynamic model presented above. Again, the trends of decreasing values along the series are observed, with the highest value obtained for C_{18}. However, the Pugh modulus ratio (G/B) for all three allotropes is almost the same (~1.15).

The fracture toughness of C_{18} (6.3 MPa·m^{½}) is between the corresponding values for diamond and lonsdaleite, while two hybrid allotropes show lower values, i.e. 5.7 and 4.4 MPa·m^{½} for *ene*-C_{21} and *yne*-C_{24}. Similar trends are also observed for Young's modulus (E) and Poisson's ratio (ν).

These trends in mechanical properties are consistent with the decrease in density and increase in openness of the structure upon introduction of C=C and C≡C bonds in *ene*-C_{21} and *yne*-C_{24} respectively.

Dynamic properties from the phonons

Other stability criteria, namely dynamic stability, were obtained by studying phonons, defined as quanta of vibrations. The phonon energy is quantized by the Planck constant h multiplied by the frequency ω, giving the phonon energy $E = (h/2\pi)\omega$. The calculations of the phonons for C_{18}, *ene*-C_{21} and *yne*-C_{24} are illustrated with the corresponding band structures shown in Fig. 3. In all three panels all frequencies are positive signaling stable systems. Marked differences between the three carbon

allotropes are observed for the highest frequencies of the optical modes. In C_{18} they culminate at $\omega \sim$ 40 THz, a magnitude observed for diamond by Raman spectroscopy [29]. In *ene*-C_{21} they culminate at $\omega_{max} \sim 42$ THz, a magnitude also observed for *ene*-like C_{10}, C_{14} [8], as well as in tetragonal C_6 with 3 tetrahedral and 3 trigonal carbons, where the flat band was attributed to antisymmetric C-C-C stretching in the allene (propadiene) molecule [30]. The phonon band structure of *yne*-C_{24}, exhibits flat bands at 70 THz, which can be assigned to C≡C characterized by much shorter distance than in *ene*-C_{21}.

Electronic band structures

The electronic band structures shown in Fig. 4 were obtained using the ASW method [17] with crystal inputs of the calculated crystal parameters from Table 1. The bands develop along the main directions of the primitive rhombohedral Brillouin zone. For the diamond-like 9R C_{18}, Fig. 4a shows an insulating behavior with a large band gap ~5eV separating the filled valence band VB from the empty conduction band CB. The energy level along the vertical line is with respect to the top of the valence band (VB), E_V. In contrast, *ene*-C_{21} is metallic-like with a band that crosses the Fermi level E_F, and the energy is now with respect to E_F. Such behavior can be explained by the delocalized nature of the π electrons resulting from the C=C bonds. Finally, *yne*-C_{24}, shows a semiconducting behavior and the zero energy is with respect to E_V. The localization of the charge at the triple C≡C bond can explain the semiconducting behavior.

Conclusions

The aim of this work was to give diamond new properties by introducing additional carbon atoms forming C=C and C≡C bonds into the rhombohedral 9R polytype C_{18}. The resulting new structures were geometry-optimized to the ground state and found to be cohesive, though less than pristine 9R diamond polytype. Like 9R C_{18}, *ene*-C_{21} and *yne*-C_{24} belong to the **cfe** topology characterizing layered SiC polytypes. From mechanical characterization, the two hybrid allotropes have been identified as ultrahard and dynamically stable. They exhibit high-frequency vibrational phonon modes close to the molecular C=C and C≡C bonds characteristic of as allene and acetylene molecules, respectively. The electronic band structures are indicative of the insulating C_{18}, metallic *ene*-C_{21} and semiconducting *yne*-C_{24}. It is suggested that such model systems are likely to help improve experimental studies of nanodiamonds for electronic and other applications.

References

[1] Comprehensive Semiconductor Science and Technology (Eds. P. Bhattacharya, R. Fornari and H. Kamimura), Elsevier, 2011.

[2] P.D. Ownby, X. Yang, J. Liu, Calculated X-ray diffraction data for diamond polytypes. *J. Am. Ceram. Soc.*, **75** (1992) 1876-1883.

[3] V.L. Deringer, G. Csányi, D.M. Proserpio, Extracting crystal chemistry from amorphous carbon structures. *ChemPhysChem*, **18** (2017) 873-877.

[4] R. Hoffmann, A. Kabanov, A. Golov, D.M. Proserpio. Homo Citans and carbon allotropes: For an ethics of citation. *Angew. Chem., Int. Ed.*, **55** (2016) 10962-10976.

[5] Y. Lin, X. Sun, D.S. Su, G. Centi, S. Perathoner, Catalysis by hybrid sp^2/sp^3 nanodiamonds and their role in the design of advanced nanocarbon materials. *Chem. Soc. Rev.*, **47** (2018) 8438-8473.

[6] Z. Zhai, N. Huang, X. Jiang, Progress in electrochemistry of hybrid diamond/sp^2-C nanostructures. *Curr. Opin. Electrochem.*, **32** (2022) 100884.

[7] M. Hu, Q. Huang, Z. Zhao, B. Xu , D. Yu, J. He, Superhard and high-strength yne-diamond semimetals. *Diam. Relat. Mater.*, **46** (2014) 15-20.

[8] S.F. Matar, V. Eyert, V.L. Solozhenko, Novel ultrahard extended hexagonal C_{10}, C_{14} and C_{18} allotropes with mixed sp^2/sp^3 hybridizations: Crystal chemistry and ab initio investigations. *C*, **9** (2023) 11.

[9] P. Hohenberg, W. Kohn, Inhomogeneous electron gas. *Phys. Rev. B*, **136** (1964) 864-871.

[10] W. Kohn, L.J. Sham, Self-consistent equations including exchange and correlation effects. *Phys. Rev. A*, **140** (1965) 1133-1138.

[11] S. Matar. « eneC_{21}-166 ». CCDC Deposition Number 2242799. Refcode LIHFAN. DOI: 10.5517/ccdc.csd.cc2f8tcx (2023).

[12] S. Matar. « yneC_{24}-166 ». CCDC Deposition Number 2242896. Refcode LIHNID DOI: 10.5517/ccdc.csd.cc2f8xh4 (2023).

[13] G. Kresse, J. Furthmüller, Efficient iterative schemes for ab initio total-energy calculations using a plane-wave basis set. *Phys. Rev. B*, **54** (1996) 11169.

[14] P.E. Blöchl, Projector augmented wave method. *Phys. Rev. B*, **50** (1994) 17953-17979.

[15] J. Perdew, K. Burke, M. Ernzerhof, The Generalized Gradient Approximation made simple. *Phys. Rev. Lett.*, **77** (1996) 3865-3868.

[16] W. Voigt, Über die Beziehung zwischen den beiden Elasticitätsconstanten isotroper Körper. *Annal. Phys.*, **274** (1889) 573-587; D.N. Blashke, Averaging of elastic constants for polycrystals. arXiv:1706.07132v2 (2017)

[17] A. Togo, I. Tanaka, First principles phonon calculations in materials science. *Scr. Mater.*, **108** (2015) 1-5.

[18] K. Momma, F. Izumi, VESTA 3 for three-dimensional visualization of crystal, volumetric and morphology data. *J. Appl. Crystallogr*., **44** (2011) 1272-1276.

[19] V. Eyert, Basic notions and applications of the augmented spherical wave method. *Int. J. Quantum Chem.*, **77** (2000) 1007-1031.

[20] R. Gaillac, P. Pullumbi, F.-X. Coudert, ELATE: an open-source online application for analysis and visualization of elastic tensors. *J. Phys.: Condens. Matter* **28** (2016) 275201.

[21] V.V. Brazhkin, V.L. Solozhenko, Myths about new ultrahard phases: Why materials that are significantly superior to diamond in elastic moduli and hardness are impossible. *J. Appl. Phys*., **125** (2019) 130901.

[22] V.A. Mukhanov, O.O. Kurakevych, V.L. Solozhenko, The interrelation between hardness and compressibility of substances and their structure and thermodynamic properties. *J. Superhard Mater.,* **30** (2008) 368-378.

[23] S.F. Matar, V.L. Solozhenko, Crystal chemistry and ab initio prediction of ultrahard rhombohedral B_2N_2 and BC_2N. *Solid State Sci.*, **118** (2021) 106667.

[24] V.L. Solozhenko, S.F. Matar, Prediction of novel ultrahard phases in the B–C–N system from first principles: Progress and problems. *Materials*, **16** (2023) 886.

[25] A.O. Lyakhov, A.R. Oganov, Evolutionary search for superhard materials: Methodology and applications to forms of carbon and TiO_2. *Phys. Rev.* B, **84** (2011) 092103.

[26] E. Mazhnik, A.R. Oganov, A model of hardness and fracture toughness of solids. *J. Appl. Phys.*, **126** (2019) 125109.

[27] X.Q. Chen, H. Niu, D. Li, Y. Li, Modeling hardness of polycrystalline materials and bulk metallic glasses. *Intermetallics* , **19** (2011) 1275-1281.

[28] N. Bindzus, T. Straasø, N. Wahlberg, J. Becker, L. Bjerg, N. Lock, A.-C. Dippel, B.B. Iversen, Experimental determination of core electron deformation in diamond. *Acta Cryst. A*, **70** (2014) 39-48.

[29] R.S. Krishnan, Raman spectrum of diamond. *Nature*, **155** (1945) 171.

[30] S.F. Matar. Crystal chemistry rationale and DFT investigations of novel hard tetragonal C_6 built from tetrahedral $C(sp^3)$ lattice embedding allene-like sp^2 linear tricarbon. ChemArxiv. 10.26434/chemrxiv-2022-3cs4s and Universal Journal of Carbon Research, in press Feb 2023 https://ojs.wiserpub.com/index.php/UJCR DOI: https://doi.org/10.37256/xxxx

Table 1 Crystal structure parameters of carbon allotropes with **cfc** topology. Values for **cfe** C_{18} are calculated for the C_{18} structure proposed by Deringer *et al*. [3].

Space group *R-3m* (No 166)	**cfe** C_{18} SACADA Database Code: 447	**cfe** *ene*-C_{21}	**cfe** *yne*-C_{24}
a, Å	2.510	2.4922	2.5935
c, Å	18.672	22.988	26.290
V_{cell}, Å^3	101.91	123.65	153.14
$<V_{atom}>$ Å^3	5.66	5.97	6.38
Density, (g/cm^3)	3.52	3.39	3.13
Shortest bonds, Å	1.54, 1.56	1.46, 1.54, 1.55	1.21, 1.56, 1.59
Atomic position	C1 (6c) 0, 0, 0.0635(0.1806) C2 (6c) 0, 0, 0.0635(0.2644) C3 (6c) 0, 0, 0.0635(0.9588)	C1 (6c) 0, 0, 0.0635 C2 (6c) 0, 0, 0.1782 C3 (6c) 0, 0, 0.24579 C4 (3a) 0, 0, 0	C1 (6c) 0, 0, 0.02267 C2 (6c) 0, 0, 0.0774 C3 (6c) 0, 0, 0.1766 C4 (6c) 0, 0, 0.2358
E_{tot}, eV	-163.43	-181.89	-204.54
E_{tot}/atom, eV	-9.079	-8.661	-8.523
E_{coh}/atom, eV	-2.479	-2.061	-1.923

Table 2 Elastic constants C_{ij} and Voigt values of bulk (B_V) and shear (G_V) moduli (all values are in GPa) of carbon allotropes with **cfc** topology.

	C_{11}	C_{12}	C_{13}	C_{33}	C_{44}	C_{66}	B_V	G_V
cfe C_{18}	1168	131	30	1288	518	459	445	516
cfe *ene*-C_{21}	1009	89	33	1423	460	420	417	479
cfe *yne*-C_{24}	794	76	21	1406	359	380	359	415

Table 3 Vickers hardness (H_V) and bulk moduli (B_0) of **cfe** carbon allotropes calculated within the framework of the thermodynamic model of hardness [22]

	Space group	$a = b$ (Å)	c (Å)	ρ (g/cm^3)	H_V (GPa)	B_0 (GPa)
C_{18} #166	*R*-3*m*	2.5104	18.672	3.523	98	444
ene-C_{21} #166	*R*-3*m*	2.4922	22.987	3.387	94	427
yne-C_{24} #166	*R*-3*m*	2.5935	26.290	3.126	87	394
Lonsdaleite	*P*6$_3$/*mmc*	2.5221*	4.1186‡	3.516	97	443
Diamond	*Fd*-3*m*	3.56661‡		3.517	98	445†

* Ref. 2

‡ Ref. 28

† Ref. 21

Table 4 Mechanical properties of **cfe** carbon allotropes: Vickers hardness (H_V), bulk modulus (B), shear modulus (G), Young's modulus (E), Poisson's ratio (ν) and fracture toughness (K_{Ic})

	H_V				B		G_V	E**	ν**	K_{Ic}‡
	T*	LO†	MO‡	CN§	B_0*	B_V				
	GPa									MPa·m$^{1/2}$
C_{18} #166	98	90	97	89	444	445	516	1117	0.082	6.3
ene-C_{21} #166	94	73	89	84	427	417	479	1039	0.084	5.7
yne-C_{24} #166	87	69	77	78	394	359	415	899	0.082	4.4
Lonsdaleite	97	90	99	94	443	432	521	1115	0.070	6.2
Diamond	98	90	100	93	445††		530††	1138	0.074	6.4

* Thermodynamic model [22]

† Lyakhov-Oganov model [25]

‡ Mazhnik-Oganov model [26]

§ Chen-Niu model [27]

** E and ν values calculated using isotropic approximation

†† Ref. 21

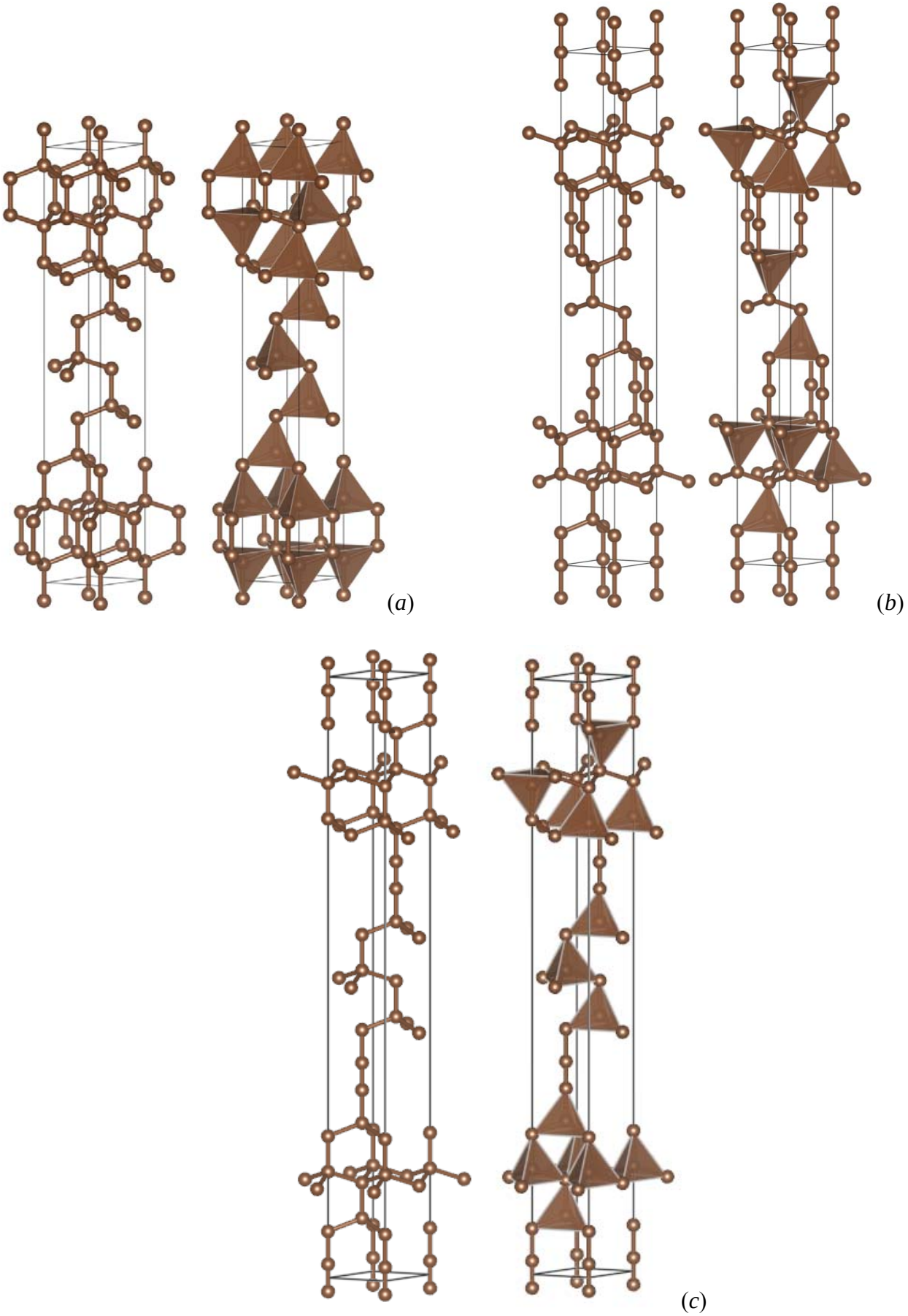

Fig. 1 Ball-and-stick (left) and tetrahedral (right) representations of crystal structures of C_{18} (*a*), *ene*-C_{21} (*b*) and *yne*-C_{24} (*c*).

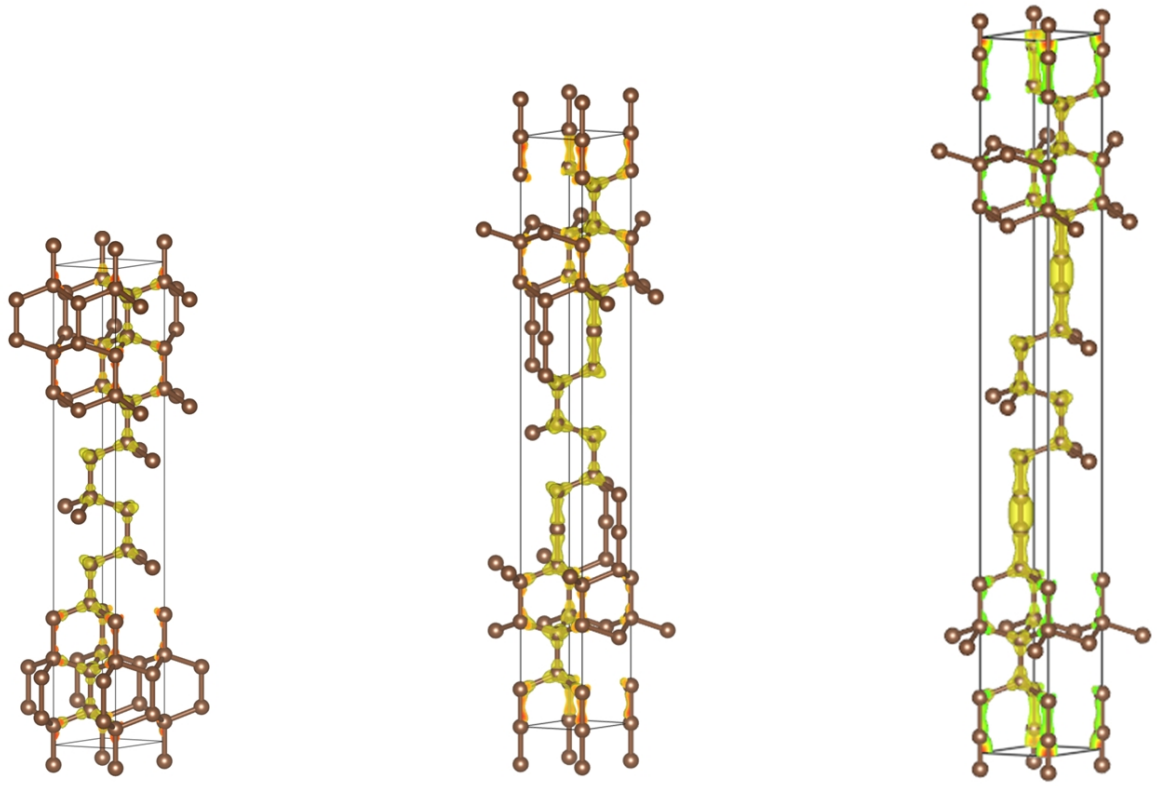

(*a*) (*b*) (*c*)

Fig. 2. Charge density projections (yellow volumes) in C_{18} (*a*), *ene*-C_{21} (*b*) and *yne*-C_{24} (*c*).

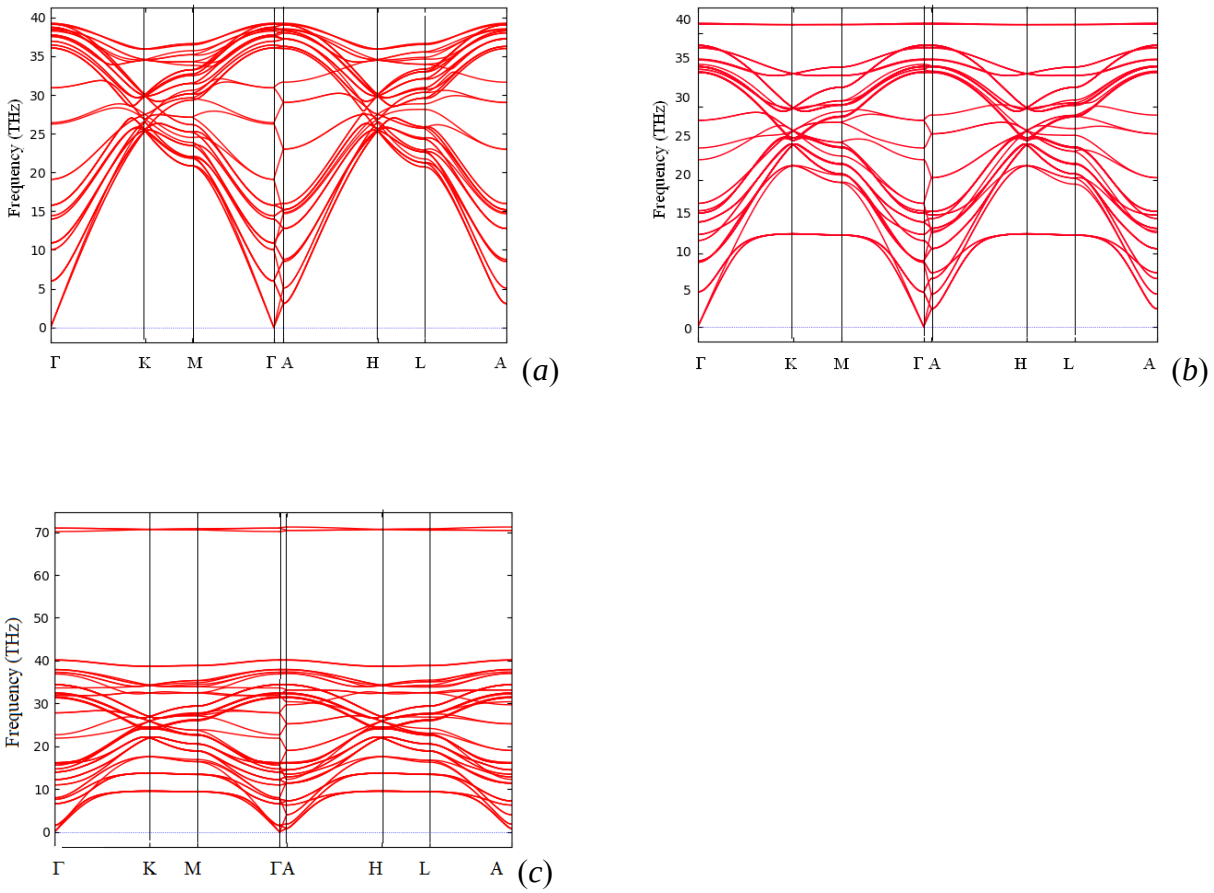

Fig. 3. Phonons band structures of C_{18} (*a*), *ene*-C_{21} (*b*) and *yne*-C_{24} (*c*).

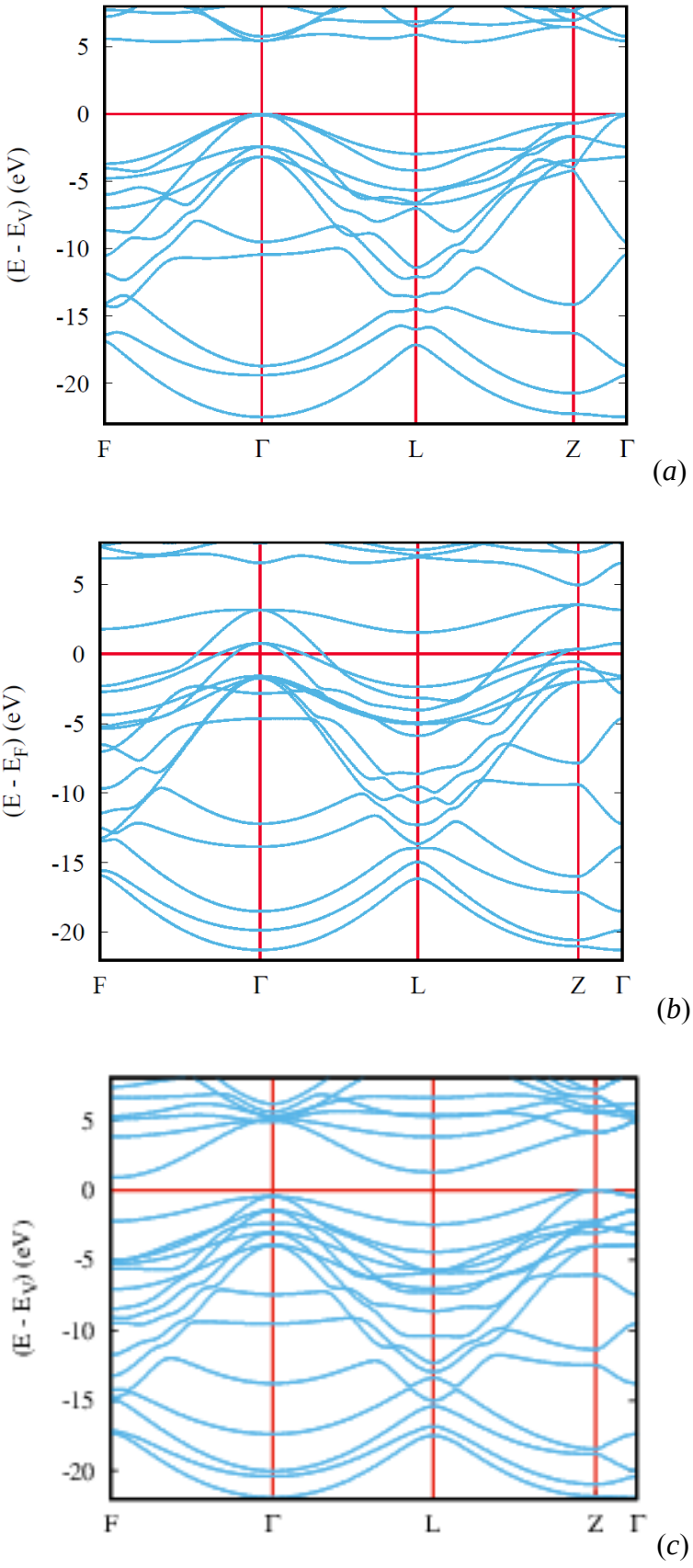

Fig. 4. Electronic band structures of C_{18} (*a*), *ene*-C_{21} (*b*) and *yne*-C_{24} (*c*).